Two-Band Whistler-Mode Waves Outside the Plasmapause: Observational Features and Theoretical Constructions

David Shklyar, Elena Titova, and Andris Lubchich

Abstract – A case study is presented of whistler waves in the frequency bands below and above half the electron gyrofrequency observed by Van Allen Probe B in the equatorial region outside the plasmapause. Based on simultaneous measurements of electron differential fluxes, we calculate the linear growth rate γ and spatial amplification factor γ/v_g (v_g is the magnitude of the group velocity) as functions of frequency and wave normal angle, taking into consideration three main cyclotron resonances. Calculated quantities, with the account of relative position of the observation point and the generation region, permit one to explain the main features of the observed spectrum. The reasons for two maxima in the dependence of the growth rate on frequency and the corresponding two-band structure in the observed spectrum are discussed.

1. Introduction

Many works have been devoted to the study of very low frequency (VLF) waves outside the plasmapause, most of which are related to the study of chorus emissions that usually exist in two frequency bands [1, 2, and references therein]. In this article, we analyze whistler waves in the VLF range in the frequency bands below and above half the electronic gyrofrequency, whose spectrum does not have a pronounced time-frequency structure typical of chorus emissions.

A detailed discussion of views concerning excitation of banded whistler waves outside the plasmapause available on the eve of Van Allen Probes era [3] may be found in [4], together with new results on this matter based on particle-in-cell simulations. Calculations of the linear growth rate for parallel propagating whistler waves were performed in [5, 6] using differential electron flux measurements by MagEIS [7] and HOPE [8] instruments on board Van Allen Probes.

This article represents a case study of the dynamic spectrum of whistler waves registered by Van Allen Probe B on 30 November 2015. Using simultaneous measurements of differential electron fluxes, we calculate the linear amplification factor for the whole frequency band of whistler waves and all angles of propagation inside the resonance cone. Assuming that the generation region is located in the equatorial region close to the observation point, we show that the features of the observed spectrum may be understood based on the calculated amplification factor considering the relative position of the generation region and the observation point, with the account of measured Poynting vector of the observed waves.

Manuscript received 7 December 2022.

David Shklyar is with the Space Research Institute of RAS, 84/32 Profsoyuznaya Street, Moscow, 117997, Russia; e-mail: david@iki.rssi.ru.

Elena Titova is with the Polar Geophysical Institute, 26a Academgorodok Street, Apatity, 184209, Russia, and the Space Research Institute of RAS, 84/32 Profsoyuznaya Street, Moscow, 117997, Russia; e-mail: lena.titova@gmail.com.

Andris Lubchich is with the Polar Geophysical Institute, 26a Academgorodok Street, Apatity, 184209, Russia; e-mail: lubchich@pgia.ru.

2. Data Presentation of the Case Study

Figure 1 shows the overview spectrogram of the wave event considered in this article. The data were taken by the Van Allen Probe B satellite on 30 November 2015 in the time interval from 14:00 UT to 15:15 UT during a moderate geomagnetic storm (D_{st} index was equal to –37 nT, and AE index was ~160 nT). During this time, the satellite was in the afternoon sector (from 14.5 MLT to 16.0 MLT) in the equatorial region, MLAT varying from 1.9° to –3.5°. The satellite moved toward lower L shells, from $L = 5$ to $L = 3.3$. Frequencies of the VLF emission increased with decreasing L in proportion to the electron gyrofrequency f_c (see Figures 1a–1c). Maximum frequencies of the order of 16 kHz were observed on $L = 3.5$ at 15:10 UT, when the satellite reached the plasmapause (see Figure 1f). VLF emissions were registered in the frequency band from $0.2\,f_c$ to $0.75\,f_c$. Two spectral maxima, below $fc/2$ and above $f_c/2$, were often observed (see, e.g., the time interval from 14:35 UT to 14:55 UT in Figures 1b and 1c). In contrast to chorus emissions, which also have two bands below and above $f_c/2$, the VLF emissions under consideration were of hiss type, and their intensities were less than that of chorus emissions [9, 10].

At frequencies $f < f_c/2$, the wave normal angles of the emissions were mostly less than 20° (see Figure 1d). At frequencies $f > f_c/2$, the wave normal angles were also small before 14:30 UT, but then larger angles up to 40° in the lower part of the upper frequency band were registered. The wave normal angles were obtained from multicomponent measurements. The magnetic planarity (not shown) exceeded 0.5 most of the time, so the wave propagation analysis can be considered reliable. We should mention that we do not consider the emissions in the frequency band from 1 kHz to 3.5 kHz that have large wave normal angles >60°. Figure 1e shows the Poynting flux polar angle θ_s for Van Allen Probe B

observations. At the beginning of the wave event, the Poynting vector of the emission under consideration was directed along the ambient magnetic field (i.e., to the north). Since at that time the satellite was in the Northern Hemisphere, this corresponds to the direction from the geomagnetic equator. Then the satellite moved to the south and crossed the equatorial region, where the wave intensity decreased substantially. After crossing the equator, the direction of the Poynting vector changed sign; thus, the waves again propagated from the equator, implying that the source of the emissions was in the equatorial region.

The wave analysis presented above was performed with the help of Autoplot browser (https://autoplot.org) using the data from the EMFISIS instrument on board Van Allen Probes [11]. The survey mode data with 6 s cadence were mainly used, although the hiss structure of the emission under discussion was verified using the waveform of the signal available in burst mode. The determination of the wave normal vector and the Poynting flux vector embedded in Autoplot is based on the methods developed in [12, 13]. The cold electron density is derived from the upper hybrid resonance frequency measured by the high-frequency receiver of the EMFISIS instrument [14].

3. Calculation of Linear Growth Rate From Electron Flux Measurements

A general expression for the linear growth rate of obliquely propagating whistler waves, together with its detailed derivation, may be found in [15]. Here we present this expression with the explanation of the main entering quantities, referring the reader to the previously mentioned article for comprehensive clarification:

$$\gamma_{\mathrm{L}} = \sum_{n=-\infty}^{\infty} \gamma_{\mathrm{L}n} \equiv \frac{\omega_c (\pi e c |E|)^2}{2 m k_{||} U} \sum_{n=-\infty}^{\infty} \int_0^{\infty} d\mu f'_{0n}(\mu) V_n^2(\mu) \tag{1}$$

Here U is the wave energy density and $|E|$ is the magnitude of the wave electric field component in the ($\mathbf{k}$, $\mathbf{B}_0$) plane perpendicular to $\mathbf{B}_0$. Here $\mathbf{k}$ is the wave normal vector, and $\mathbf{B}_0$ is the ambient magnetic field. In the expressions above and further on, $\omega = 2\pi f$ is the wave angular frequency; k is the magnitude of the wave normal vector; $k_{||} = k \cos\theta$ is the component of the wave vector along the ambient magnetic field; θ is the wave normal angle (i.e., the angle between $\mathbf{k}$ and $\mathbf{B}_0$); e and m are the magnitude of electron charge and the electron mass, respectively; $\omega_c = 2\pi f_c$ and $\omega_p = 2\pi f_p$ are magnitudes of the angular electron cyclotron frequency and electron plasma frequency, respectively; and c is the speed of light. Relation (1) is valid under the assumption that the wave dispersion properties are determined by the bulk cold plasma, while the wave growth or damping is determined by low-density energetic electrons that can interact resonantly with the wave but do not affect its dispersion properties.

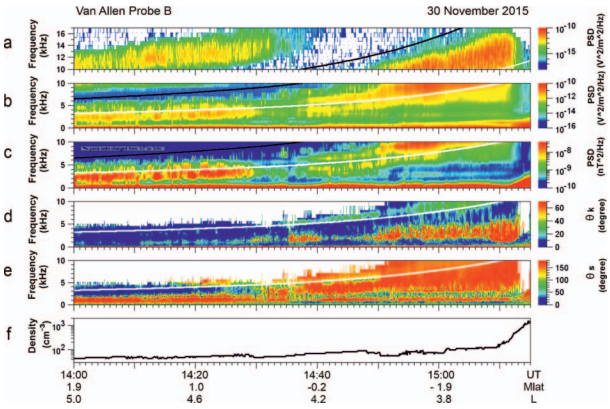

Figure 1. Overview spectrogram of VLF emissions recorded by Van Allen Probe B on 30 November 2015. (a) Electric power spectral density in the frequency range from 10 kHz to 17 kHz; electric (b) and magnetic (c) power spectral density in the frequency range from 0.01 kHz to 10 kHz; polar angles of wave normal (d) and Poynting flux (e). The black and white lines indicate the electron gyrofrequency f_c and half the gyrofrequency $f_c/2$, respectively. (f) Cold plasma density.

Expression (1) contains the sum over all cyclotron resonances, although the main contribution to the growth rate is made by the first cyclotron resonance $n = 1$, Landau resonance $n = 0$, and cyclotron resonance $n = -1$, whose contribution to the growth rate we will take into account in numerical calculations. The unperturbed distribution function f_0 is assumed to be the function of particle constants of the motion in the absence of the wave field, namely, kinetic energy $w = mv^2/2$ and magnetic momentum $\mu = mv_{\perp}^2/2\omega_c$. The quantities f'_{0n} and V_n that enter (1) are given by

$$f'_{0n} = \left(\frac{\partial f_0}{\partial w} + \frac{n}{\omega}\frac{\partial f_0}{\partial \mu}\right)_{w = m v_{rn}^2/2 + \mu\omega_c} \quad ; \quad v_{rn} = \frac{\omega - n\omega_c}{k_{||}} \tag{2}$$

$$V_n = \left(\frac{n\omega_c}{k_{\perp}c} + \frac{v_{rn}}{c}a_{||}\right) J_n(\rho) - \frac{i\rho\omega_c}{k_{\perp}c} a_{\phi} J'_n(\rho) \; ; \; \rho = k_{\perp}\sqrt{\frac{2\mu}{m\omega_c}} \tag{3}$$

In (3), $J_n(\rho)$ and $J'_n(\rho)$ are the Bessel function of the first kind of the order n and its derivative with respect to ρ, respectively, and $a_{||}$ and a_{ϕ} are the polarization coefficients (see [15]).

Expression (1) is written in CGS units, which also apply to the distribution function f_0. This quantity is related to the differential flux J measured in practical units $1/(\mathrm{cm}^2 \cdot \mathrm{s} \cdot \mathrm{sr} \cdot \mathrm{keV})$ by the relation [16]

$$f_{\mathrm{CGS}} = 1.62 \cdot 10^{-37} \frac{J}{W} \tag{4}$$

where W is particle energy in keV. Formulas (1)–(4), together with the differential electron flux measured by the Van Allen Probe instruments, permit one to calculate the linear growth rate in the whole frequency band of whistler waves and for all allowed wave normal

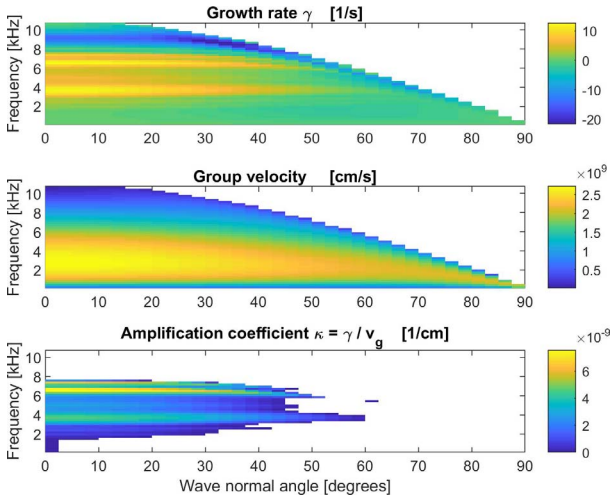

Figure 2. Growth rate (upper panel), group velocity (middle panel), and amplification factor (lower panel) on (θ, f) planes calculated from differential electron fluxes measured at 14:42:45 UT.

angles inside the resonance cone. If we exclude frequencies $f << f_c$ and take into account that in the whole spatial area related to Figure 1 the ratio $f_p/f_c \geq 5$, we find that the resonance energies fall within the range from units to several tens of keV covered by the HOPE instrument on Van Allen Probes. One should keep in mind that for a fixed wave normal angle, the resonant velocity at the first cyclotron resonance, which makes the main contribution to the growth rate away from the resonance cone, decreases quite fast with increasing frequency. Therefore, in general, higher-frequency waves are excited by lower-energy particles and vice versa. (We should mention that including differential fluxes at higher energies measured by the MagEIS instrument does not change the results substantially.) Below we present the results of calculations using the differential electron fluxed measured on 30 November 2015 at 14:42:45 UT and the corresponding plasma parameters also available from measurements. Since the measured fluxes are not symmetrical with respect to the pitch angle $\alpha = \pi/2$ and since the waves propagating in different directions with respect to the ambient magnetic field interact with particles from different domains of pitch angles, the growth rates for waves propagating in different directions, although having the same $|\cos\theta|$, appear to be different.

Before presenting the results of numerical calculations of the growth rate, an important remark is in order. In the data, differential fluxes and, thus, the distribution function are determined on a rectangular (α, w) grid, while the corresponding (μ, w) grid is not rectangular since $\mu = w \sin^2\alpha/\omega_c$. In the MATLAB environment in which the calculations were carried out, a non-rectangular grid is not acceptable either for two-dimensional interpolation or for calculating line-by-line or column-by-column partial derivatives. Therefore, the calculated line-by-line partial derivative with respect to energy is the derivative at a constant pitch angle, while formula (1) includes a derivative at a constant μ. These derivatives are connected by the relation

$$\left(\frac{\partial f_0}{\partial w}\right)_\mu = \left(\frac{\partial f_0}{\partial w}\right)_\alpha - \left(\frac{\partial f_0}{\partial \mu}\right)_w \frac{\sin^2\alpha}{\omega_c}$$

which was used to numerically calculate the partial derivative of the distribution function with respect to energy at a constant μ.

Figure 2 shows the growth rate γ on the (θ, f)-plane for whistler waves at Van Allen Probe B position at the moment of time indicated above (i.e., 14:42:45 UT) and the corresponding amplification factor γ/v_g with the negative values removed. At that time, the satellite was on $L = 4.2$, at a latitude of –0.4°, and the electron cyclotron frequency f_c was 10.9 kHz. The most striking feature of the growth rate is the existence of two frequency maxima, below and above half the gyrofrequency, with lower values of the growth rate between them. This feature persists in the amplification factor, although it is modified by the group velocity shown in the middle panel, which, at small θ, has maximum at $f \simeq f_c/4$ and decreases with increasing wave normal angle.

The VLF spectrum detected on an electrical antenna at 14:42:45 UT is shown in Figure 3a. It also has two maxima at frequencies well matched to local maxima of the amplification factor and the growth rate shown in Figures 3b and 3c, respectively. A decrease in the group velocity v_g with increasing frequency significantly increases the amplification factor of VLF waves at frequencies above $f_c/2$ as compared to lower-frequency maxima. One can see from Figure 2b that at frequencies $> f_c/2$, intense VLF waves can be generated in the range of wave normal angles up to 30° or even 40°, which is consistent with observations (see Figure 1d). We should stress that the existence of two unstable bands is revealed not only for oblique but also for parallel propagation, that is, in the frame of validity of classical results of [17], further used by many authors (e.g., [18]). The instability criterion found in [17] reads $\omega/\omega_c < A/(1 + A)$, where A is anisotropy of the distribution determined in [17, equation (2.20)]. As was mentioned in [17], this criterion gives a singly connected unstable range only if A does not depend on frequency. In the general case, when the quantity A depends on frequency, the above given inequality becomes transcendental and may have solution in multiple frequency bands.

4. Discussion and Summary of Results

When waves are excited due to electron cyclotron instability in the equatorial region of the magnetosphere and are observed at very low latitudes, as takes place in the case under discussion, the peculiarities of the observed spectrum should be closely related to the local amplification factor. Simultaneous wave and particle measurements by Van Allen Probes provide a unique opportunity to perform such a comparison. To

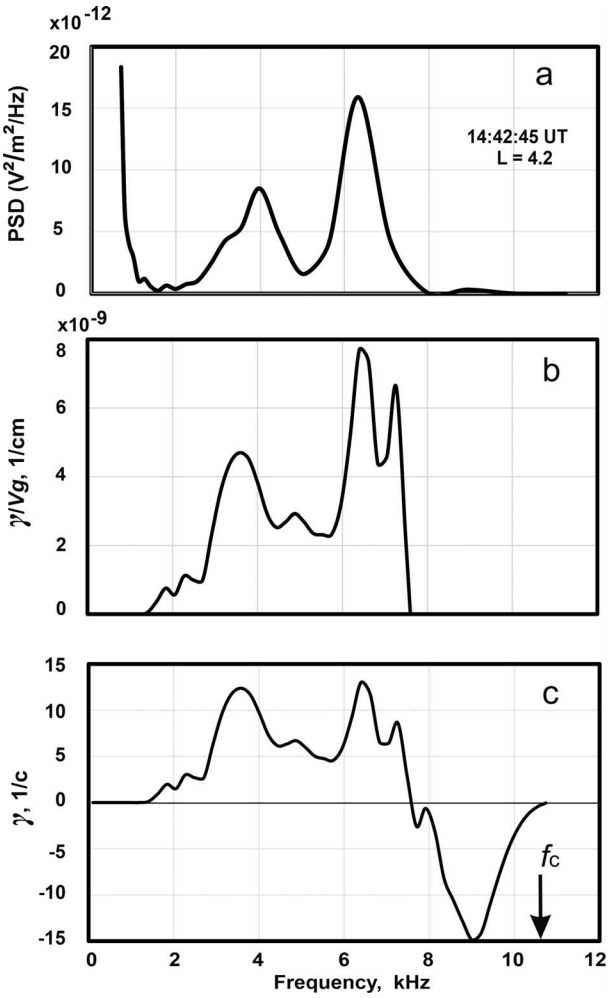

Figure 3. Comparison of the spectrum of VLF waves detected by Van Allen Probe B on the electric antenna at 14:42:45 UT (a) with the amplification coefficient (b; only positive values are shown) and the growth rate (c) of whistler waves as functions of frequency for parallel propagating (from north to south) waves.

this end, we have calculated the linear growth rate γ and the amplification factor γ/v_g as functions of frequency and wave normal angle based on the measurements of electron differential fluxes by the Van Allen Probe B satellite. We have compared the obtained amplification factor with spectral characteristics of simultaneously observed whistler emissions and found quite good correspondence between them. In the wave event under discussion, the maxima below and above $f_c/2$ in the observed wave spectra and in the growth rate and the amplification factor were present quite often and regularly so in the time interval from 14:35 UT to 14:55 UT.

The most remarkable feature of the observed spectrum and the calculated growth rate is the existence of two spectral maxima, below and above half the electron gyrofrequency. We have found the peculiarity of the electron distribution function responsible for this feature (although we have not determined the reason for this peculiarity to appear), which consists of a very sharp drop in the distribution function with increasing energy in the energy range that makes the main contribution to the growth rate of whistler waves at half the gyrofrequency. This feature is revealed in the analysis of the distribution function determined by the differential electron fluxes. To understand qualitatively why such a dependence of the distribution function leads to a significant decrease in the growth rate at frequencies near $f_c/2$, we first notice that the growth rate is determined by the "competition" between the decrease in the distribution function with increasing energy and the increase, if exists, in the distribution function with increasing magnetic momentum [see (1)]. To make a contribution to the growth rate, the particle energy should be larger than the parallel resonant energy $w_{r||} = mv_{r1}^2/2$, and this contribution increases with increasing μ and thus the total energy. (In this reasoning, we consider parallel propagation and therefore only the first cyclotron resonance). Thus, the range of particle energies that makes the main contribution to γ spreads from $w_{r||}$ to a few $w_{r||}$. In the case under discussion, for $f = f_c/2$, $w_{r||} = 1.24$ keV. A further increase of μ and thus of particle energy is accompanied by an overall decrease in the number of resonant particles. As the examination of the distribution function shows, just in this range of energies, the derivative $\partial f_0/\partial w$ has the largest-magnitude negative values, which leads to suppression of the growth rate at the corresponding frequencies.

Observation and analysis of whistler waves in two frequency bands were presented in a number of papers (e.g., [19]). Our results differ from those reported in [19], first, in the propagation properties of the discussed emission, in particular, relatively small wave normal angles in both frequency bands, and, second, in the way of calculating the growth rate directly from the measured distribution without approximating it by model analytical functions.

In sum, based on simultaneous wave and particle measurements by Van Allen Probe B in the equatorial region outside the plasmapause, we have shown that the observed VLF spectrum is consistent with the local linear amplification factor calculated from the measured particle fluxes. The consideration performed gives a hint to the understanding of the long-standing problem of the origin of two frequency bands in VLF spectrograms.

5. Acknowledgments

The data used in this study are available from the EMFISIS website at http://emfisis.physics.uiowa.edu/data/index and from https://cdaweb.gsfc.nasa.gov. The authors are grateful to the Van Allen Probe team for free access to the data. The work of D. R. Shklyar and E. E. Titova was supported by the Russian Science Foundation (project no. 22-22-00135).

6. References

1. A. Artemyev, O. Agapitov, D. Mourenas, V. Krasnoselskikh, V. Shastun, and F. Mozer, "Oblique Whistler-Mode Waves in the Earth's Inner Magnetosphere: Energy Distribution, Origins, and Role in Radiation Belt Dynamics," *Space Science Reviews*, **200**, April 2016, pp. 261-355.
2. J. Li, J. Bortnik, X. An, W. Li, V. Angelopoulos, et al., "Origin of Two-Band Chorus in the Radiation Belt of Earth," *Nature Communications*, **10**, October 2019, pp. 1-9.
3. N. Fox and J. Burch (eds.), *Van Allen Probes Mission*, New York, Springer, 2014.
4. K. Liu, S. P. Gary, and D. Winske, "Excitation of Banded Whistler Waves in the Magnetosphere," *Geophysical Research Letters*, **38**, 2011, L14108.
5. A. A. Lubchich, A. G. Demekhov, E. E. Titova, and A. G. Yahnin, "Amplitude-Frequency Characteristics of Ion-Cyclotron and Whistler-Mode Waves From Van Allen Probes Data," *Geomagnetism and Aeronomy*, **57**, 2017, pp. 40-50.
6. Z. He, L. Chen, X. Liu, H. Zhu, S. Liu, Z. Gao, and Y. Cao, "Local Generation of High-Frequency Plasmaspheric Hiss Observed by Van Allen Probes," *Geophysical Research Letters*, **46**, February 2019, pp. 1141-1148.
7. J. B. Blake, P. A. Carranza, S. G. Claudepierre, J. H. Clemmons, W. R. J. Crain, et al., "The Magnetic Electron Ion Spectrometer (MagEIS) Instruments Aboard the Radiation Belt Storm Probes (RBSP) Spacecraft," *Space Science Reviews*, **179**, 2013, pp. 383-421.
8. H. O. Funsten, R. M. Skoug, A. A. Guthrie, E. A. MacDonald, J. R. Baldonado, et al., "Helium, Oxygen, Proton, and Electron (HOPE) Mass Spectrometer for the Radiation Belt Storm Probes Mission," *Space Science Reviews*, **179**, 2013, pp. 423-48.
9. O. V. Agapitov, D. Mourenas, A. V. Artemyev, F. S. Mozer, G. Hospodarsky, J. Bonnell, and V. Krasnoselskikh, "Synthetic Empirical Chorus Wave Model From Combined Van Allen Probes and Cluster Statistics," *Journal of Geophysical Research: Space Physics*, **123**, 2018, pp. 297-314.
10. H. Aryan, J. Bortnik, N.P. Meredith, R.B. Horne, D. G. Sibeck, and M. A. Balikhin, "Multi-Parameter Chorus and Plasmaspheric Hiss Wave Models," *Journal of Geophysical Research: Space Physics*, **126**, 2021, e2020JA028403.
11. C. A. Kletzing, W. S. Kurth, M. Acuna, R. J. MacDowall, R. B. Torbert, et al., "The Electric and Magnetic Field Instrument Suite and Integrated Science (EMFISIS) on RBSP," *Space Science Reviews*, **179**, November 2013, 1–4, pp. 127-181.
12. O. Santolik, M. Parrot, and F. Lefeuvre, "Singular Value Decomposition Methods for Wave Propagation Analysis," *Radio Science*, **38**, 1, 2003, p. 1010.
13. O. Santolik, J. S. Pickett, D. A. Gurnett, J. D. Menietti, B. T. Tsurutani, and O. Verkhoglyadova, "Survey of Poynting Fux of Whistler Mode Chorus in the Outer Zone," *Journal of Geophysical Research: Space Physics*, **115**, A7, A00F13, 2010, pp. 1-13.
14. W. S. Kurth, S. De Pascuale, J. B. Faden, C. A. Kletzing, G. B. Hospodarsky, S. Thaller, and J. R. Wygant, "Electron Densities Inferred From Plasma Wave Spectra Obtained by the Waves Instrument on Van Allen Probes," *Journal of Geophysical Research: Space Physics*, **20**, 2015, pp. 904-914.
15. D. Shklyar and H. Matsumoto, "Oblique Whistler-Mode Waves in the Inhomogeneous Magnetospheric Plasma: Resonant Interactions With Energetic Charged Particles," *Surveys in Geophysics*, **30**, 2009, pp. 55-104.
16. D. R. Shklyar, E. E. Titovaa, J. Manninend, and T. V. Romantsova, "Whistler Growth Rates in the Magnetosphere According to Measurements of Energetic Electron Fluxes on the Van Allen Probe A Satellite," *Geomagnetism and Aeronomy*, **60**, 2020, pp. 46-57.
17. C. F. Kennel and H. E. Petschek, "Limit of Stably Trapped Particle Fluxes," *Journal of Geophysical Research*, **71**, 1, 1966, pp. 1-28.
18. P. Hosseini, M. Golkowski, and V. Harid, "Remote Sensing of Radiation Belt Energetic Electrons Using Lightning Triggered Upper Band Chorus," *Geophysical Research Letters*, **46**, 2019, pp. 37-47.
19. O. Santolik, D. A. Gurnett, J. S. Pickett, S. Grimald, P. M. E. Décreau, et al., "Wave-Particle Interactions in the Equatorial Source Region of Whistler-Mode Emissions," *Journal of Geophysical Research: Space Physics*, **115**, A8, 2010, p. A00F16.